Hindawi
Geofluids
Volume 2023, Article ID 2766524, 13 pages
https://doi.org/10.1155/2023/2766524

Research Article

Fine Detection and Analysis of Hidden Karst in Wellsite with Quasi-Three-Dimensional TDEM Based on Lateral Constraint

Bin Wu,[1,2,3] **Yunping Liao**,[1] **Hongkai Chen**,[3] **Lichuan Chen**,[1] **Shicong Ren**,[1] **Shihong Xiao**,[4] **Yunjian Yang**,[5] **Yong Yang**,[1] **and Haiyou Peng**[1,6]

[1]*Technology Innovation Center of Geohazards Automatic Monitoring, Ministry of Natural Resources (Chongqing Institute of Geology and Mineral Resources), Chongqing 401120, China*
[2]*Chongqing Industry Polytechnic College, Chongqing 401120, China*
[3]*Chongqing Jiaotong University, Chongqing 400074, China*
[4]*Chongqing Changnan Gas Transmission and Distribution Co., Ltd, Chongqing 401123, China*
[5]*BGP Inc. Zhuozhou, Hebei 072750, China*
[6]*School of Civil Engineering, Chongqing University, Chongqing 401144, China*

Correspondence should be addressed to Yunping Liao; liaoyunping@cqdky.com

Received 13 June 2023; Revised 13 October 2023; Accepted 2 November 2023; Published 22 November 2023

Academic Editor: Zhiqiang Fan

Considering that karst caves, underground rivers, and dissolution fractures in shallow carbonate formation in the Sichuan Basin are extremely developed, leakage, failure and plugging difficulties are easy to occur in the drilling process. The TDEM was used to carry out the exploration of hidden karst geological bodies in well QM2, and the quasi-three-dimensional inversion based on lateral constrain was used to invert the TDEM data. Three NW trending anomalous bands were identified in the lower Triassic Jialingjiang Formation within the range of drilling, consisting of seven relatively low-resistivity anomalous zones. Under the guidance of TDEM quasi-three-dimensional inversion resistivity data, the low-resistivity karst development area is avoided, and the specific drilling location of well QM2 is determined. No karst cave and underground river were drilled in the later drilling process of well QM2, as well as no instability phenomenon occurred. It indicates that the TDEM detection results are consistent with the actual drilling, and the quasi-three-dimensional TDEM inversion interpretation data based on lateral constraints is reliable and can accurately detect the buried karst in the wellsite.

1. Introduction

Sichuan Basin is a typical multiphase tectonic superposition basin, longitudinally developing three major accumulation systems, namely, the Mesozoic continental accumulation system, Upper Paleozoic Marine accumulation system, and Lower Paleozoic Marine accumulation system. The effective exploration area is $18 \times 10^4\,km^2$, and the total natural gas resources are $38.84 \times 10^{12}\,m^3$. Among them, unconventional natural gas (shale gas, coalbed methane, etc.) is $21.74 \times 10^{12}\,m^3$, which is the main target of future natural gas development. Due to multistage tectonic cycles, unconventional natural gas resources mainly occur in the Upper Ordovician Wufeng-Lower Silurian Longmaxi Formation and the Upper Permian Longtan Formation, and drilling zones are mainly located in the Permian and Triassic carbonate strata. Due to the influence of topography, structure, climate, and other factors, carbonate formation is extremely developed. It is very easy to drill beaded karst carves, caves, and corrosion fractures in the process of drilling, which will cause drilling accidents such as leakage, drilling loss, and fish dropping [1, 2]. For example, serious drilling fluid loss occurred when well ZY1 in the Qianjiang area of Chongqing was drilled to 54 m, with a loss of $2154\,m^3$. In addition, 101 times of well leakage occurred during drilling in Daye Formation and Maokou Formation (0-730 m), with a loss of $25342.07\,m^3$, lasting for 43 days, which seriously affected drilling efficiency, drilling quality, and engineering safety. During the handling process of drilling

accidents, imaging is used to detect the leakage site, which is mainly caused by karst caves and corrosion fractures (Figure 1). Therefore, in view of the problems of karst caves, fractures, and underground rivers in the shallow carbonate formation of the Sichuan Basin, which are easy to leak and difficult to stop during the drilling process, the application of TDEM electrical exploration technology to detect the development of hidden karst in the wellsite and its surrounding areas will provide a basis for the selection of drilling well location, the selection of construction technology, and the evaluation of engineering safety.

2. TDEM Detection Principle and Inversion Method

2.1. TDEM Karst Detection Principle. At present, a large number of scholars have made detailed discussions and studies on the formation mechanism of karst geological bodies [3, 4], but how to accurately identify karst caves, underground rivers, cracks, and other hidden karst geological bodies is still a hot issue. Geophysical exploration is an economical, rapid, nondestructive, and efficient means, among which high-density electrical method, geological radar method, audio magnetotelluric method, time domain electromagnetic method, and surface nuclear magnetic resonance method are widely used in the detection of adverse geological bodies (karst caves, underground rivers, cracks, underground goaf, faults, and geological disaster investigation) [5–11]. With the digitization and intellectualization of instruments and the development of processing and interpretation technology, the scope of geological problems that can be solved is constantly expanding [12–15]. The time domain electromagnetic method (TDEM) uses a grounded conductor or ungrounded loop to send a pulsed electromagnetic field underground. After the primary field is disconnected, the electromagnetic conductivity distribution characteristics of the medium are detected by observing and studying the change of secondary eddy current field with time [16–18]. Nabighian vividly described the detection principle of TDEM using the "smoke ring theory" [19]. The transient response can be approximately equivalent to a current ring that diffuses underground. The current ring is the "smoke ring" blown out by the transmission loop, which has the same shape as the transmission loop and diffuses outward and downward as the delay increases (Figure 2). According to this principle, the transient response measured on the surface over time can be transformed into a function curve of resistivity changing with depth, thus achieving transient electromagnetic detection of underground abnormal geological bodies. For uniform half-space conditions, an analytical expression for the transient response of the central loop can be obtained:

$$H_z = \frac{I}{2a}\left[\left(1-\frac{3}{u^2}\right)\varphi(u)+3\left(\frac{\sqrt{(2/\pi)}e^{-u^2/2}}{u}\right)\right], \quad (1)$$

$$\dot{H}_z = \frac{3I\rho}{\mu_0 a^3}\left[\varphi(u)-\sqrt{\frac{2}{\pi}}ue^{-u^2/2}\left(1+\frac{1}{3}u^2\right)\right]. \quad (2)$$

$H_z^{\bullet}$ represents the time derivative of Hz, I represents the emission current, ρ represents the resistivity, a represents the radius of the loop line, and $u = 2\pi a/\tau$, $\tau = 2\pi\sqrt{2\rho t/\mu_0}$, and $\varphi(u)$ are error functions.

The secondary attenuation curve reflects the characteristics of the resistivity changing with time. Due to the diffusion of the earth's secondary field to the deep underground over time, the attenuation curve also reflects the characteristics of the earth's resistivity changing with depth. Through inversion interpretation, the curve of the earth's resistivity changing with depth can be obtained.

TDEM is a method of generating an excited electromagnetic field (Figure 2 (a)) by using an ungrounded loop or a long grounded wire to supply a bipolar pulse current. Under the excitation of this electromagnetic field, a conductive geological body is induced to generate a vortex current. Due to the nonlinearity of conductive geological bodies, the pulse current jumps from peak to zero, and the primary magnetic field immediately disappears, while the eddy current does not immediately disappear. There is a transient process, and the speed of this process is related to the electrical parameters of the conductor. The better the conductivity of the geological body, the smaller the heat loss of the eddy current, and the longer the transient process. This eddy current transient process forms a corresponding transient magnetic field in space (Figure 2 (c)). Observing the transient magnetic field on the ground during the pulse current shutdown period, that is, observing the secondary magnetic field (Figure 2 (b)), can reveal the existence of underground abnormal geological bodies, thus determining the electrical structure and spatial distribution of underground conductors.

This method is an artificial source secondary field method, which has advantages such as high data signal-to-noise ratio, no interference from the primary field, less affected by topographic relief in high-resistivity surrounding rock areas, strong ability to penetrate high-resistivity overburden, and large detection depth. In recent years, it has been favored by karst researchers and applied to karst detection [20–22]. Since TDEM observes the electromotive force data in the time domain, it is necessary to obtain the resistivity in the depth domain through inversion and then interpret related geological problems. Therefore, inversion is the basis for the correct understanding of geological bodies.

2.2. TDEM Inversion Method. The data processing method of TDEM is usually to convert the induced electromotive force into the early, late, or whole period apparent resistivity [19, 23–26] and then use the apparent resistivity for inversion. For example, one-dimensional semiquantitative inversion methods like "floating thin plate interpretation method" and "smoke loop" interpretation method based on the horizontal-layered medium model are introduced, which have the characteristics of fast inversion without the initial model. However, these methods are based on single-point one-dimensional inversion or imaging, the continuity of the inversion section is poor, only approximate geological understanding can be obtained, the late signal is weak, the deep area is greatly affected by noise, and the geological body is not easy to implement. Although the second and third inversions of

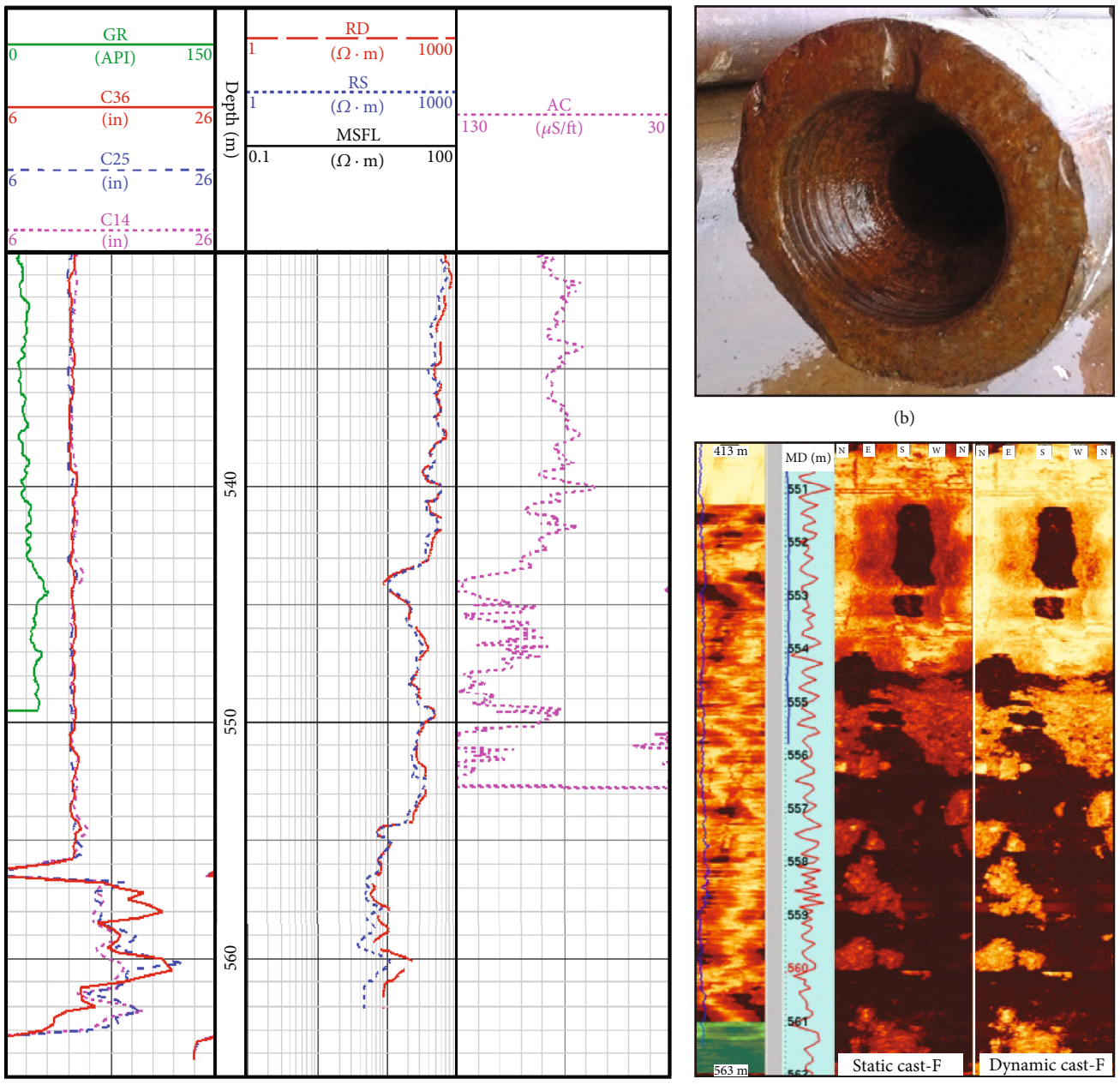

Figure 1: Logging interpretation diagram of well ZY1 leakage imaging. (a) Feature diagram of well ZY1 conventional logging. (b) Fracture diagram of drill pipe. (c) Circumferential acoustic scanning tool (CAST-F) imaging logging, showing dark clumps at 554.0 ~ 562.0 m, indicating that large corrosion holes were developed in this section, resulting in fluid loss.

TDEM have made great progress [12, 16, 27–31], they have not been popularized and applied due to the large amount of calculation and the limitation of computing platform. Therefore, considering the poor continuity, strong heterogeneity, and difficult identification of hidden karst geological body, based on the regularized one-dimensional inversion, this paper introduced horizontal constraint inversion to simulate three-dimensional inversion, so as to suppress the unreasonable phenomena of inversion model mutation caused by single-point noise and effectively identify hidden karst geological body in the wellsite.

2.3. Quasi-Three-Dimensional Inversion with Lateral Constraints. In order to more accurately characterize the hidden karst geological body, this optimization one-dimensional inversion is based on the Marquette method, and the longitudinal roughness of the model is added to the objective function. Then, the lateral constraint is regularized and added to the inversion objective function. In other words, the model difference between each measurement point and its several adjacent point was added to the inversion objective function, and the collected induced electromotive force is directly inverted and fitted [32–35]. By the quasi-three-dimensional inversion based

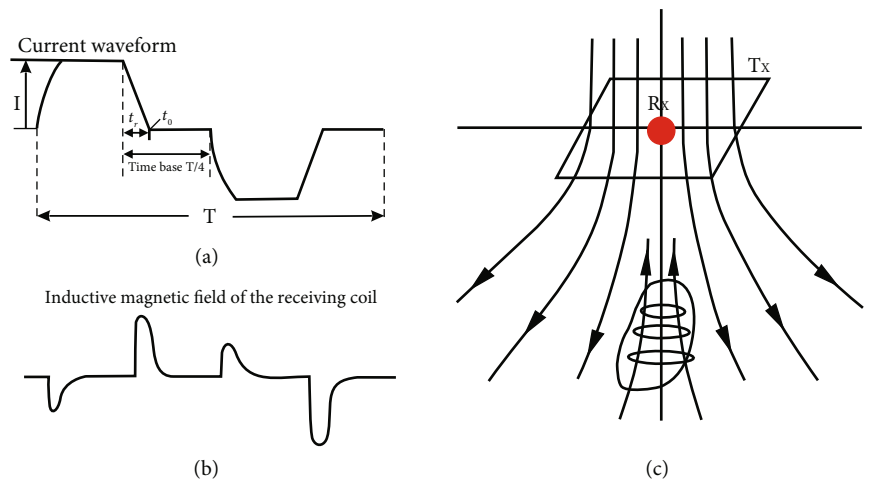

Figure 2: Schematic diagram of the TDEM principle.

on the lateral constraint, the unreasonable phenomena of inversion model mutation caused by single-point noise can be suppressed, and the hidden karst geological body in the wellsite can be identified effectively. The detail of the algorithm of the quasi-three-dimensional inversion based on the lateral constraints is described as follows [36, 37].

Based on the basic idea of lateral constraint, the geoelectric model of measuring points is inverted by using the distance-weighted lateral constraint of p measuring points which are the nearest to measuring points within radius r, so as to realize the transverse constraint quasi-three-dimensional inversion of TDEM data. There are setting n measuring points which are numbered in a certain sequence, and each measuring point has m attenuation delay. The electromagnetic data of these n measuring points can be expressed as

$$d = [d_{11}, d_{12}, \cdots, d_{1m}, \cdots, d_{i1}, d_{i2}, \cdots, d_{im}, \cdots, d_{n1}, d_{n2}, \cdots, d_{nm}]^T. \tag{3}$$

Assuming that the inversion model has k layers and only considering the conductivity σ of each layer, the total model of n measurement points can be expressed as

$$m = [\sigma_{11}, \sigma_{12}, \cdots, \sigma_{1k}, \cdots, \quad \sigma_{i1}, \sigma_{i2}, \cdots, \sigma_{ik}, \cdots, \quad \sigma_{n1}, \sigma_{n2}, \cdots, \sigma_{nk}]^T. \tag{4}$$

Then, the quasi-three-dimensional inversion objective function with distance-weighted lateral constraints can be written as

$$\begin{aligned}\phi = {} & [F(m) - d]^T C^{-1} [F(m) - d] + k_v (E_v m)^T \times (E_v m) \\ & + k_h \sum_{i=1}^{p} (E_{h,i} m)^T D_i^{-1} (E_{h,i} m),\end{aligned} \tag{5}$$

where F is the forward operator; $\boldsymbol{C}$ is the covariance matrix, which is used to weight the fitting of observation data based on errors. k_v and k_h are the longitudinal and transverse constraint factors, respectively. E_v is the longitudinal first-order difference matrix of each measuring point model. $\boldsymbol{E}_{h,i}$ is the first-order difference matrix of transverse constraint for the ith adjacent points of each measuring point (if the ith adjacent point of a measuring point does not exist, all the row elements corresponding to the measuring point in $\boldsymbol{E}_{h,i}$ are zero); $\boldsymbol{D}_i$ is the transverse constraint distance-weighted matrix of the ith adjacent points. $E_v m$ and $E_{h,i} m$ represent the longitudinal roughness of the model corresponding to measuring points and the transverse roughness of the ith adjacent point, respectively. E_v, $E_{h,i}$, and D_i can be expressed as

$$E_V = \begin{bmatrix} -1 & 1 & 0 & \cdots & & & 0 \\ 0 & -1 & 1 & 0 & \cdots & & 0 \\ & & & \cdots & & & \\ 0 & \cdots & & \cdots & 0 & -1 & 1 \end{bmatrix}_{[n\times(k-1)]\times(n\times k)}, \tag{6}$$

$$E_{h,i} = \begin{bmatrix} -1 & 0 & \cdots & 1 & 0 & \cdots & 0 \\ 0 & -1 & 0 & \cdots & 1 & \cdots & 0 \\ & & & \cdots & & & \\ 0 & \cdots & 0 & 1 & 0 & \cdots & -1 \end{bmatrix}_{(n\times k)\times(n\times k)}, \tag{7}$$

$$D_i^{-1} = \begin{bmatrix} \dfrac{1}{r_{1,i}} & 0 & \cdots & & & 0 \\ 0 & \dfrac{1}{r_{1,i}} & 0 & \cdots & & 0 \\ & & \cdots & & & \\ & & & 0 & \dfrac{1}{r_{n,i}} & 0 \\ 0 & \cdots & & & 0 & \dfrac{1}{r_{n,i}} \end{bmatrix}_{(n\times k)\times(n\times k)}, \tag{8}$$

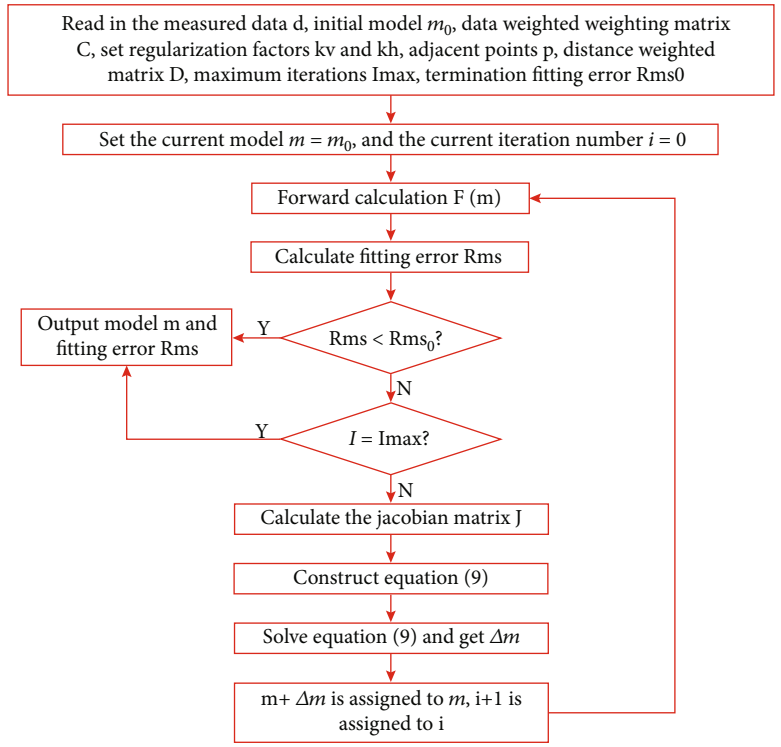

Figure 3: The inversion process diagram.

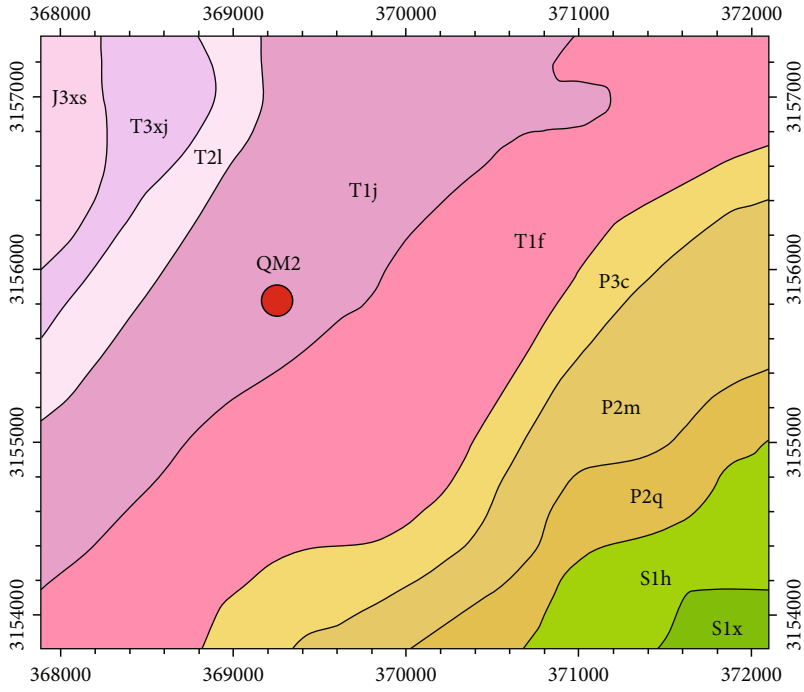

Figure 4: Geological map of the survey area.

where $r_{n,i}$ represents the distance between the nth measuring point and its ith adjacent point. During actual data processing, a minimum distance r_0 should be set, and when $r_{ni} < r_0$, let r_0 replace r_{ni}. The difference of geoelectric models between each measuring point and its pth adjacent measuring points is added into Formula (5) successively to conduct lateral constraints on the model; then, the minimum of the objective function is obtained; that is, the least square solution of transverse smoothing constraint can be obtained, thus achieving the transverse constraint quasi-three-dimensional inversion.

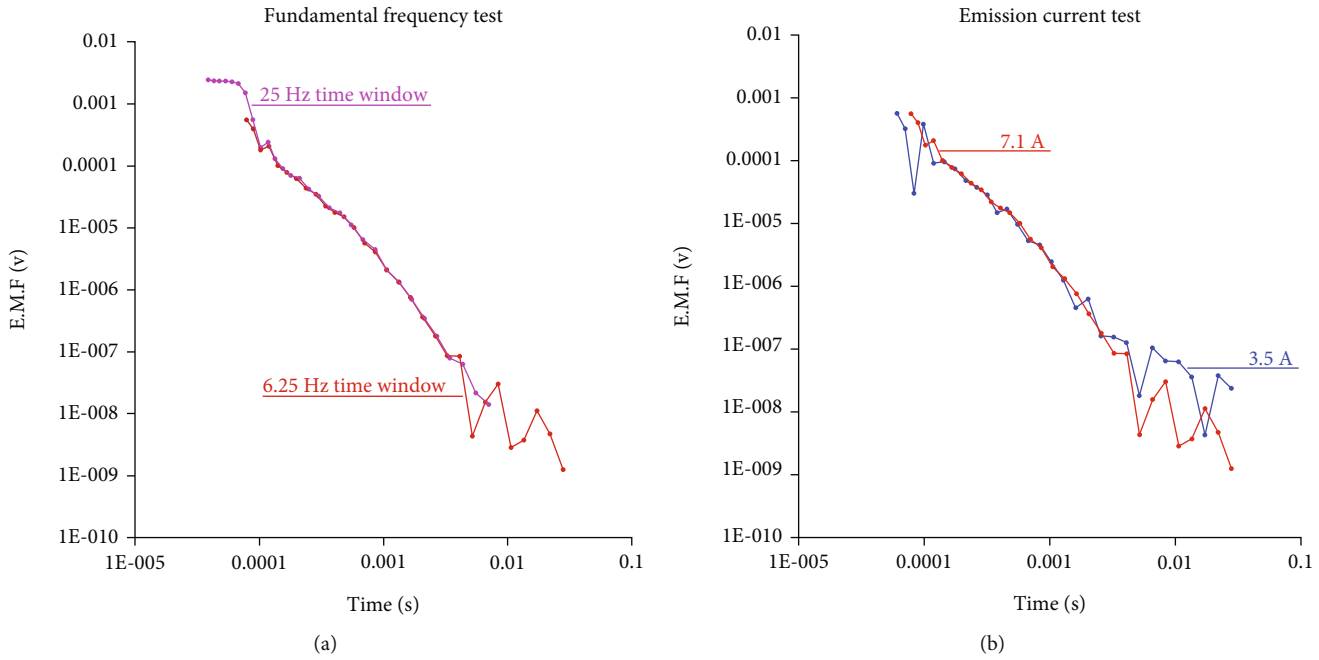

Figure 5: Comparison curves of TDEM acquisition parameters. (a) Attenuation curves of different time windows. (b) Attenuation curves of different currents.

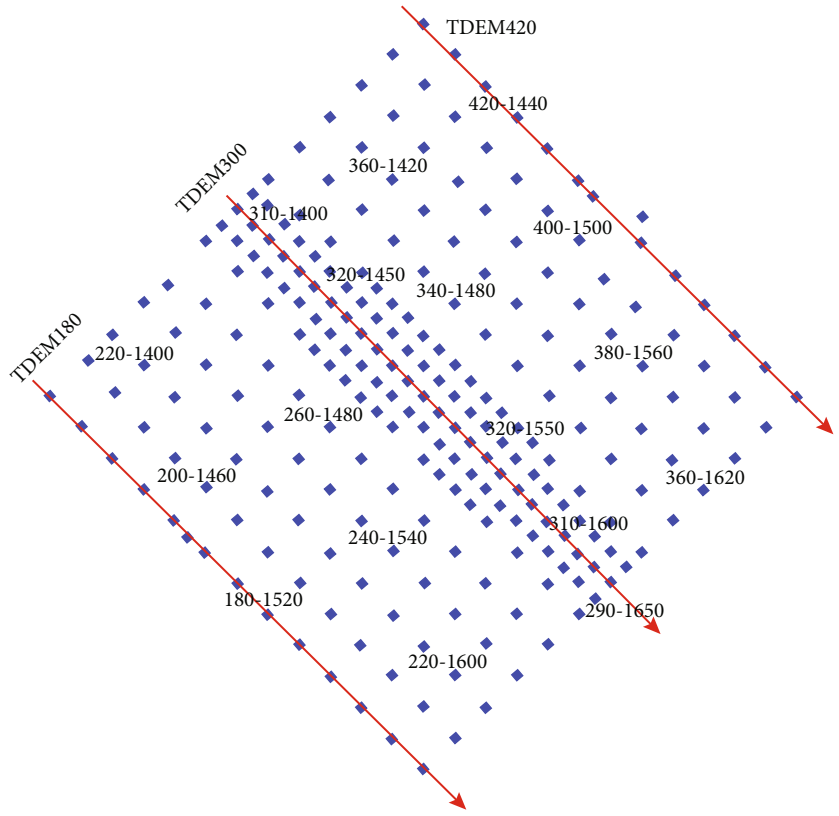

Figure 6: Distribution of TDEM measuring points in well QM2.

For solving the minimum value of the objective function in the lateral constraint quasi-three-dimensional inversion, the Gaussian-Newton method is used to solve equation (5). Let m_0 be the initial value of the model, $\triangle m$ is the model correction amount, and F is expanded in the first order at m_0, and the objective function is used to take the derivative

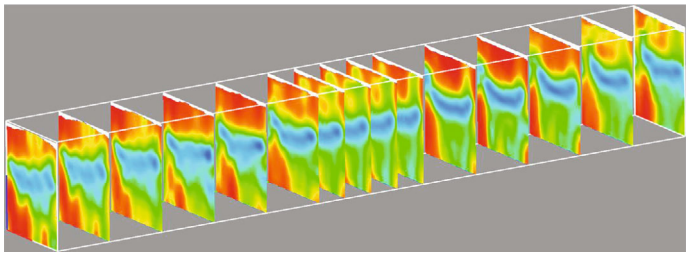

Figure 7: TDEM180-420 line inversion resistivity imaging of well QM2 (low resistance anomalies in blue, high resistance anomalies in red).

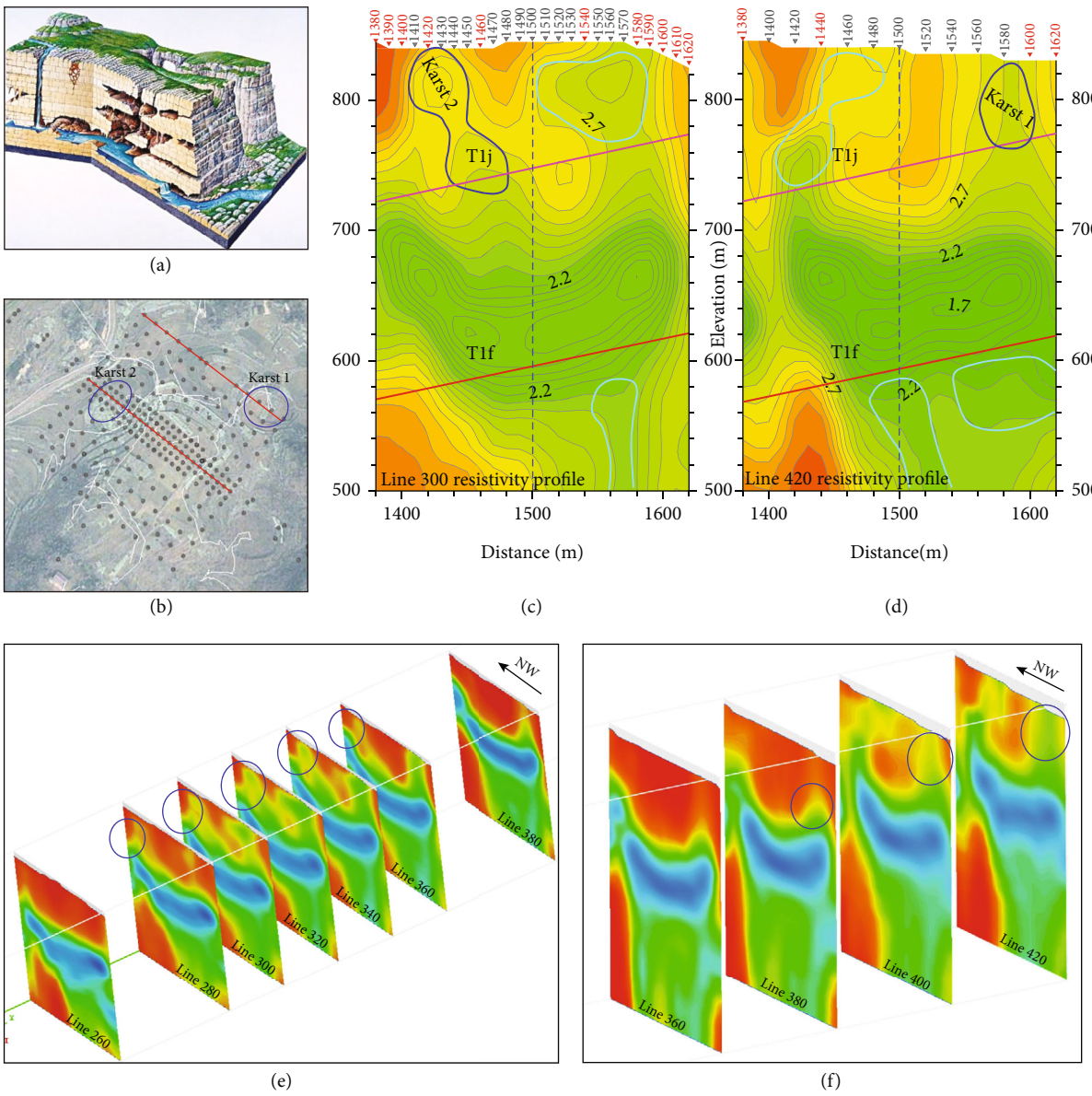

Figure 8: Karst development characteristics of TDEM resistivity inversion profile in well QM2 (the area delineated by the blue line is a low-resistivity anomaly; Figure 6(e) shows that the farther away from the collapse, the higher the resistivity and the smaller the anomaly scale. Figure 6(e) shows that the closer to the collapse pit, the lower the resistivity and the larger the anomaly scale).

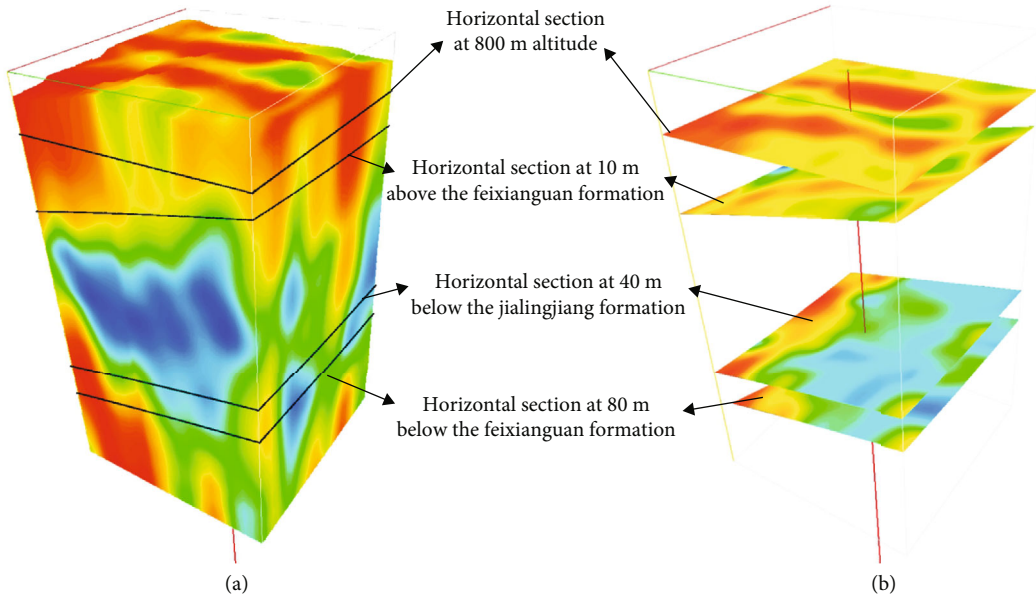

Figure 9: Results of quasi-three-dimensional inversion interpretation ((a) three-dimensional resistivity data volume and (b) resistivity slices at different layers).

of $\triangle m$ (set the derivative to 0) and obtain the solution formula for the correction of the Gaussian-Newton method as follows:

$$\left[J^T C^{-1} J + k_V E_V^T E_V + k_h \sum_{i=1}^{p} \left(E_{h,i}^T D_i E_{h,i}\right)\right] \Delta m = J^T C^{-1}[d - F(m_0)] - k_V E_V^T E_V m_0 - k_h \sum_{i=1}^{p} \left(E_{h,i}^T D_i E_{h,i} m_0\right). \tag{9}$$

In equation (9), J is the forward function and the corresponding model Jacobian diagonal matrix, which contains $n \times m \times k$ nonzero elements. Then, $\triangle m$ can be solved by equation (9), and the revised model $m = m_0 + \Delta m$ can be obtained. Then, m is assigned to m_0, and the final inversion result can be obtained by iterating repeatedly to reach the preset fitting error or the maximum number of iterations. The inversion process diagram is shown in Figure 3.

3. TDEM Data Acquisition

3.1. Geological Background. The study area is located in the Songzao area of Qijiang, Chongqing. It is a northwest-inclined monoclinic structure with a stable formation. The rock strike is N20°~30°E, and the inclination is 10°~45° (Figure 4). From southeast to northwest, the stratigraphic age changes successively, and the Silurian, Permian, and Triassic strata are exposed on the surface, where Jialingjiang Formation and Feixianguan Formation in Triassic are carbonate formation, mainly composed of gray limestone and dolomite. The drilling hole is located in the Jialingjiang Formation.

3.2. Optimizing Acquisition Parameter. This study applied a Protem transient instrument for data acquisition, used a 400 m*400 m large loop device, and conducted a fundamental frequency test and emission current test. Two fundamental frequencies, 25 Hz and 6.25 Hz, were selected for the fundamental frequency test. The 25 Hz time window is generally forward, while the 6.25 Hz time window is generally backward (Figure 5(a)). The shape of attenuation curve in overlapping time window is the same. The early signal of attenuation curve in the 25 Hz time window is saturated, while the delay is longer in the 6.25 Hz time window. The current test is conducted to compare 3.5 A current and 7.1 A current (Figure 5(b)). Compared with 3.5 A, 7.1 A can effectively improve the signal-to-noise ratio. Therefore, according to test results, the parameters are determined as a fundamental frequency of 6.25 Hz and a current of 7.1 A.

4. Results and Discussion

4.1. Results. The drilling hole is located in the area of carbonate formation. In order to reduce the risk of drilling engineering; find out the distribution of shallow surface karst cave, underground river, and fracture zone; and evaluate the stability of the drilling wellsite, 15 TDEM survey lines are deployed in and around the wellsite with drilling well QM2 location as center, external point distance of 20 m and line distance of 20 m. The distance between points and lines in the central area is 10 m, with a total line length of 8.13 km and 243 points (Figure 6). The TDEM300 line is the line passing through the well, perpendicular to formation inclination. Based on the results of quasi-three-dimensional inversion, it is shown that the resistivity inversion profile features among multiple TDEM survey lines have good consistency (Figure 7). The high and low-resistivity anomalies

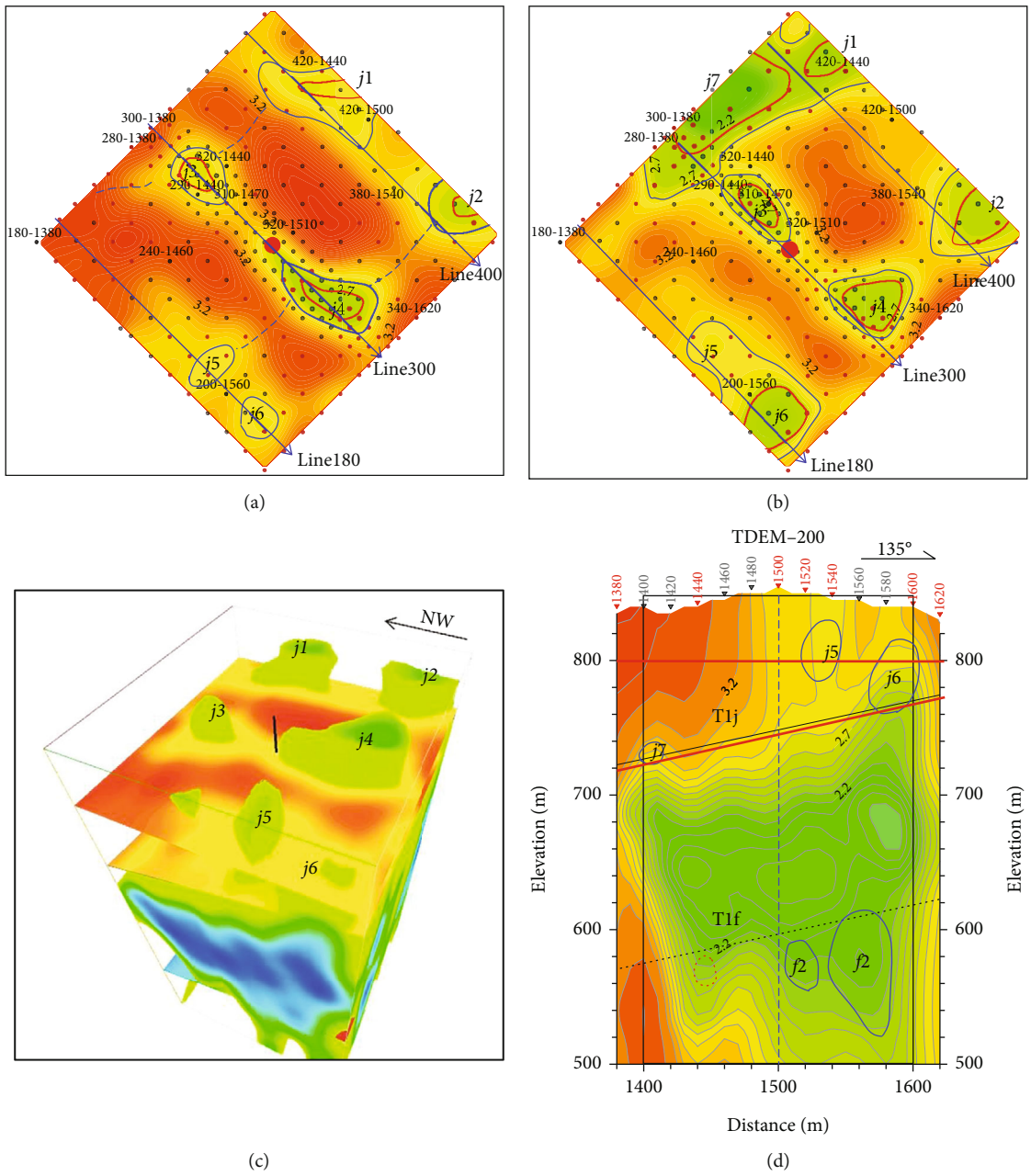

Figure 10: Continued.

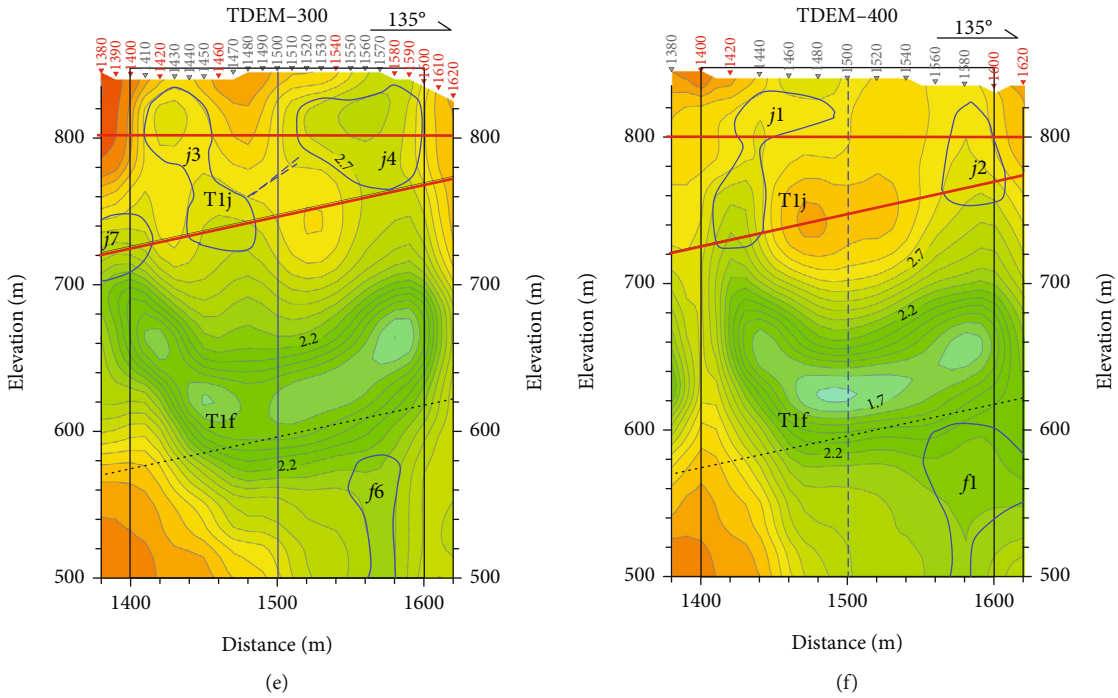

Figure 10: Evaluation map of TDEM quasi-three-dimensional resistivity inversion results in well QM2, in which low-resistivity anomalies are marked with blue lines. (a) Horizontal section at 800 m altitude; (b) stratigraphic slice at the bottom of Jialingjiang formation is 10 m upward; (c) three-dimensional display of low resistance anomaly characteristics of Jialingjiang Formation; (d) line 200 TDEM inversion profile; (e) line 300 TDEM inversion profile; (f) line 400 TDEM inversion profile.

are obvious, which can offer a basis for the analysis of karst geological bodies.

4.2. Discussion

4.2.1. Karst Characteristics of TDEM Profile. The well QM2 is located in the karst landform development area. The quasi-three-dimensional transient electromagnetic inversion results based on lateral constraints show that no obvious shallow blind area is formed in the inversion profile of each survey line, which truly reflects the variation of formation resistivity at different depths in well QM2. According to the karst development characteristics in the karst landform (Figure 8), karst caves and underground rivers are distributed in a string of beads. Previous studies have shown that the filled and unfilled karst caves in carbonate formation would show different resistivity characteristics. The filled location generally presents low resistivity, while the unfilled location presents extremely high resistivity because of air, and the karst cave filled by water presents low resistivity. Based on this, the interpretation of formation development characteristics in the area of well QM2 is carried out. In the resistivity inversion profile, the overall characteristics of high resistivity-low resistivity-high resistivity are displayed from shallow to deep, where the middle-upper part is Lower Triassic Jialingjiang Formation limestone dolomite strata, with high-resistivity upper surface of inversion profile. The middle part is Lower Triassic Feixianguan Formation member 5 marl strata, with low-resistivity upper surface of inversion profile. The bottom part is Lower Triassic Feixianguan Formation member 5 oolitic limestone strata, with relatively high-resistivity upper surface of inversion profile (Figures 8(c) and 8(d)). Therefore, according to quasi-three-dimensional inversion results, the karst collapse in Lower Triassic Jialingjiang Formation limestone dolomite high-resistivity strata is a relatively low-resistivity anomaly (Figures 8(c) and 8(d)). The position near the karst collapse center presents lower resistivity, with a larger anomaly scale, and the karst collapse center is offset at different depths (Figures 8(e) and 8(f)). No. 1 and No. 2 are visible karst caves filled with Quaternary sediments. In addition, the local groundwater level is relatively high, and if karst develops underground, it must be filled by groundwater. Therefore, it is speculated that the above local abnormal traps with low resistance and contours are caused by the decrease of resistivity in the karst development area of the Feixianguan Formation after water filling, and the development of karst cracks in the area with blue coils.

4.2.2. Karst Development Characteristics of Well QM2. According to the TDEM quasi-three-dimensional inversion results of well QM2, the Jialingjiang Formation shows several relatively low-resistivity anomalies within 200 m × 200 m of the wellsite (Figure 9). In order to determine the optimal drilling location of well QM2, the development characteristics of karst collapse within the range of the wellsite were analyzed and evaluated. In vertical direction, the Jialingjiang Formation was sliced horizontally at an altitude of 800 meters, and the stratigraphic slices were made 10 meters up the bottom of the Jialingjiang Formation, founding three NW abnormal stripes and seven relatively low-resistivity anomalies (Figure 10). TDEM180, 200, and 240 lines are the first

relatively low anomaly zone composed of j5 and j6 abnormal zones; TDEM280~340 lines are the second relatively low-resistivity anomaly zone composed of j7, j3, and j4 abnormal zones; TDEM400 and 420 lines are the third relatively low-resistivity zone composed of j1 and j2 abnormal zones. Drilling well placement is difficult in these areas. Therefore, according to quasi-three-dimensional inversion results, the drilling location of well QM2 is selected between j3 and j4 high-resistivity zones, with no obvious low-resistivity anomalies, which can ensure the safety of the drilling platform and reduce the probability of drilling karst caves and underground rivers. Although the Feixianguan Formation has low resistivity and abnormal development in depth, these areas themselves are low-resistivity strata developed by shale and marl and are presumed to be water-filled fracture development zones, which will not cause instability damage to the drilling platform. Therefore, it is necessary to strengthen the observation and adjustment of mud density during drilling. No karst cave or under river was drilled in the later drilling of well QM2, and no instability phenomenon occurred, indicating that the quasi-three-dimensional TDEM inversion interpretation data based on lateral constraints has high reliability and can be used for evaluating the stability of drilling platforms and guiding the layout of drilling wells.

5. Conclusion

(1) Considering that karst caves, corrosion fractures, and underground rivers in the shallow carbonate formation of the Sichuan Basin are extremely developed, resulting in leakage and failure during the drilling process, the electric exploration technology of TDEM is used to construct the quasi-three-dimensional inversion method with distance-weighted adjacent point lateral constraints, which provides a reliable method for the detection of hidden karst in the wellsite and its surrounding areas

(2) Aiming at the problem of difficult identification of hidden karst geological bodies in the Qijiang area, the TDEM electrical exploration, priority acquisition parameters, and quasi-three-dimensional inversion method were introduced to accurately identify three NW anomaly bands developed within the range of drilling platform, and the low-resistivity karst development area can be avoided, so that the drilling location of well QM2 is determined. No karst cave or underground river is drilled in the later drilling of well QM2, as well as no instability occurring on the drilling platform. It indicates that the quasi-three-dimensional TDEM inversion interpretation data based on lateral constraints is reliable

(3) The combination of transient electromagnetic method and quasi-three-dimensional inversion technology provides a novel approach for evaluating the stability of drilling platforms in carbonate rock-developed areas. This method enables better continuity of inversion results and allows for more intuitive observation and analysis of the spatial distribution characteristics of karst anomalies. It facilitates the overall analysis of the spatial distribution patterns and interrelationships of karst anomalies, so it helps to comprehensively evaluate the potential risks caused by karst development

(4) The quasi-three-dimensional inversion technology based on lateral constraints effectively solves the problem of poor lateral continuity in the one-dimensional inversion profile of transient electromagnetic waves, demonstrating the effectiveness of this technology in detecting karst. Therefore, in order to more accurately identify hidden karst geological bodies, further practical research needs to be carried out based on actual data, especially in combination with spatial constraint inversion (applying lateral constraints along and perpendicular to the survey line), which is an important development direction of this technology

Data Availability

The data used to support the findings of this study are included within the article.

Disclosure

The "Fine detection and analysis of hidden Karst in wellsite with quasi-three-dimensional TDEM based on lateral constraint" as a preprint has previously been published (B. Wu, Y.P. Liao, L.C. Chen, et al. 2023 doi:10.21203/rs.3.rs-2903333/v1).

Conflicts of Interest

The author declares that he and his coauthors have no conflicts of interest.

Acknowledgments

This research was supported in part by the Chongqing Industry Polytechnic College Doctoral Fund Project under Grant No. 2023GZYBSZK1-08; in part by the National Natural Science Foundation of Chongqing under Grant Nos. cstc2021jcyj-msxmX1039, CSTB2022NSCQ-MSX 1433, and CSTB2022NSCQ-MSX1466; and in part by the National Key R&D Program of China (No. 2021YFB 3901403).

References

[1] I. Mohanty, R. Nagendran, L. Bisht et al., "Development of SQUID based TDEM system and its utilization for field survey at Tumallapalle, Andhra Pradesh, India," *Journal of Applied Geophysics*, vol. 204, article 104746, 2022.

[2] F. L. Zheng, Z. Zhou, C. D. Cai et al., "Analysis of the effect of combining microgravity and microdynamic methods for the detection of hidden karst: take a shale gas drilling platform in Changning as an example," *Progress in Geophysics*, vol. 38, no. 2, pp. 967–976, 2023.

[3] A. I. Ammar, M. Gomaa, and K. A. Kamal, "Applying of SP, DC-resistivity, DC-TDIP and TDEM soundings in high saline coastal aquifer," *Heliyon*, vol. 7, no. 7, article e07617, 2021.

[4] J. M. Yang, H. C. Wang, and C. Sha, "An analysis of karst exploration based on opposing coils transient electromagnetic method," *Geophysical and Geochemical Exploration*, vol. 42, no. 4, pp. 846–850, 2018.

[5] J. H. Chang, G. Q. Xue, and R. Malekian, "A comparison of surface-to-coal mine roadway TEM and surface TEM responses to water-enriched bodies," *IEEE Access*, vol. 7, pp. 167320–167328, 2019.

[6] C. T. Yu, W. Y. Chen, X. Zhang, and K. X. Lei, "Review and challenges in the geophysical mapping of coal mine water structure," *Geofluids*, vol. 2022, Article ID 4578072, 14 pages, 2022.

[7] F. Huang, D. Wang, Y. Feng, and M. Zhang, "Prediction of the collapse region induced by a concealed karst cave above a deep highway tunnel," *Advances in Civil Engineering*, vol. 2020, Article ID 8825262, 14 pages, 2020.

[8] A. Ziadi, N. T. Hariga, and J. Tarhouni, "Use of time-domain electromagnetic (TDEM) method to investigate seawater intrusion in the Lebna coastal aquifer of eastern Cap Bon, Tunisia," *Arabian Journal of Geosciences*, vol. 10, no. 22, pp. 492–492, 2017.

[9] H. El-Kaliouby, "Mapping sea water intrusion in coastal area using time-domain electromagnetic method with different loop dimensions," *Journal of Applied Geophysics*, vol. 175, article 103963, 2020.

[10] V. Kaminski, D. D. Massa, and A. Viezzoli, "Joint inversions of two VTEM surveys using quasi-3D TDEM and 3D magnetic inversion algorithms," *Exploration Geophysics*, vol. 47, no. 4, pp. 260–268, 2016.

[11] F. Shaaban, A. Taha, A. Othman, A. L. Ayman, and E. Q. Gad, "An integrated geoinformatics and hydrogeophysical approach to assess and characterize the alluvial aquifer of Wadi Dawqah, southwestern Saudi Arabia," *Environmental Earth Sciences*, vol. 81, no. 9, pp. 1–13, 2022.

[12] J. L. Cheng, J. J. Xue, J. Zhou, Y. Dong, and L. F. Wen, "2.5-D inversion of advanced detection transient electromagnetic method in full space," *IEEE Access*, vol. 8, pp. 4972–4979, 2020.

[13] N. Ramasamy and I. Mohanty, "Characterization of TDEM system with SQUID and fluxgate magnetometers for geophysical applications," *IEEE Transactions on Applied Superconductivity*, vol. 30, no. 2, pp. 1–8, 2020.

[14] P. Huerta, P. Carrasco-García, I. Armenteros, C. Recio, J. Carrasco-García, and E. Rodríguez-Jiménez, "TDEM soundings as a tool to determine seasonal variations of groundwater salinity (Villafáfila Lakes, Spain)," *Water*, vol. 14, no. 15, p. 2402, 2022.

[15] P. Francesca, R. Adamantia, and G. Alberto, "A comparative analysis of three computational- intelligence metaheuristic methods for the optimization of TDEM data," *Pure and Applied Geophysics*, vol. 179, no. 10, pp. 3727–3749, 2022.

[16] G. Q. Xue, H. Li, Y. M. He, J. Xue, and X. Wu, "Development of the inversion method for transient electromagnetic data," *IEEE Access*, vol. 8, pp. 146172–146181, 2020.

[17] P. A. Reninger, G. Martelet, E. Lasseur et al., "Geological environment of karst within chalk using airborne time domain electromagnetic data cross-interpreted with boreholes," *Journal of Applied Geophysics*, vol. 106, pp. 173–186, 2014.

[18] F. Amato, F. Pace, A. Vergnano, and C. Comina, "TDEM prospections for inland groundwater exploration in semiarid climate, Island of Fogo, Cape Verde," *Journal of Applied Geophysics*, vol. 184, article 104242, 2021.

[19] M. N. Nabighian, "Quasi-static transient response of a conducting half-space an approximate representation," *Geophysics*, vol. 44, no. 10, pp. 1700–1705, 1979.

[20] C. Roberto, G. A. Luis, and F. Carlos, "Implicit finite-difference time-domain schemes for TDEM modeling in three dimensions," *Geophysics*, vol. 87, no. 5, pp. E347–E358, 2022.

[21] Y. J. Yang, Z. X. He, X. B. Wang, and W. F. Luo, "A discussion on layer response characters of AMT, TEM and VES and joint inversion," *Progress in Geophysics*, vol. 23, no. 5, pp. 1550–1555, 2008.

[22] J. Chen, Y. Zhang, and T. Lin, "Transient electromagnetic machine learning inversion based on pseudo wave field data," *IEEE Transactions on Geoscience and Remote Sensing*, vol. 60, pp. 1–10, 2022.

[23] G. Nesrine, J. H. Faten, K. Dhekra, B. Sihem, and G. Hakim, "Enhancing the knowledge of the deep reservoirs structuring in the Takelsa basin (northeastern Tunisia) using an integrated geophysical approach," *Arabian Journal of Geosciences*, vol. 15, no. 3, pp. 1–16, 2022.

[24] F. Ghanem, A. H. Al, and E. Al-Tarazi, "The use of electrical resistivity tomography and time domain electromagnetic methods to investigate the superficial deposits at Al al-Bayt University, Jordan as a case study," *Indonesian Journal on Geoscience*, vol. 9, no. 3, pp. 355–369, 2022.

[25] X. Sun, Y. Wang, X. Yang, and Y. B. Wang, "Three- dimensional transient electromagnetic inversion with optimal transport," *Journal of Inverse and Ill-Posed Problems*, vol. 30, no. 4, pp. 549–565, 2022.

[26] G. G. Javier, P. S. Daniel, C. G. Pedro et al., "Time-domain electromagnetics as a geophysical tool in hydrogeological exploitation projects in Mesozoic formations," *Applied Sciences-Basel*, vol. 12, no. 17, p. 8655, 2022.

[27] S. C. Li, Y. J. Liu, R. H. Peng, P. Guo, J. X. An, and L. Huang, "Research on the influencing factors of transient electromagnetic method on the detection of hidden karst," *Progress in Geophysics*, vol. 37, no. 1, pp. 397–412, 2022.

[28] A. P. Afanasenkov and D. V. Yakovlev, "Application of electrical prospecting methods to petroleum exploration on the northern margin of the Siberian platform," *Russian Geology and Geophysics*, vol. 159, no. 7, pp. 827–845, 2018.

[29] J. Wu, Q. Zhi, X. Deng et al., "Deep gold exploration with SQUID TEM in the Qingchengzi Orefield, Eastern Liaoning, Northeast China," *Minerals*, vol. 12, no. 1, pp. 102–112, 2022.

[30] M. R. Asif, T. S. Bording, P. K. Maurya et al., "A neural network-based hybrid framework for least-squares inversion of transient electromagnetic data," *IEEE Transactions on Geoscience Electronics*, vol. 60, no. 1, pp. 1–10, 2022.

[31] M. S. Alhumimidi, "An integrated approach for identification of seawater intrusion in coastal region: a case study of northwestern Saudi Arabia," *Journal of King Saud University Science*, vol. 32, no. 7, pp. 3187–3194, 2020.

[32] Y. Si, M. Li, Y. Liu, and W. Guo, "One-dimensional constrained inversion study of TEM and application in coal goafs' detection," *Open Geosciences*, vol. 12, no. 1, pp. 1533–1540, 2020.

[33] A. Mohamed, A. Othman, W. F. Galal, and A. Abdelrady, "Integrated geophysical approach of groundwater potential in Wadi Ranyah, Saudi Arabia, using gravity, electrical resistivity, and remote-sensing techniques," *Remote Sensing*, vol. 15, no. 7, p. 1808, 2023.

[34] P. Daniel, C. Javier, C. Pedro, and H. P. Luis, "Deep TDEM study for structural and mining purposes: a case study of the

Barbastro Saline-Evaporitic Formation, Spain," *Applied Sciences-Basel*, vol. 13, no. 11, pp. 6385–6395, 2023.

[35] S. Qaysi, S. S. Alharbi, and M. M. Elwaheidi, "Hydrogeophysical characterization of the Southern Red Sea coastal aquifer, Saudi Arabia, using time-domain electromagnetic method," *Human and Ecological Risk Assessment*, vol. 29, no. 2, pp. 449–462, 2023.

[36] Y. J. Yang, X. B. Wang, X. J. Liu, X. L. Mi, and L. Mao, "A three-dimensional transient electromagnetic data inversion method based on a time-frequency transformation," *Applied Geophysics*, vol. 17, no. 3, pp. 361–376, 2020.

[37] B. Wu, Y. P. Liao, H. K. Chen et al., "Fine detection and analysis of hidden Karst in wellsite with quasi-three-dimensional TDEM based on lateral constraint," *Research Square*, 2023.